Global Gene Deletion Analysis Exploring Yeast Filamentous Growth

Owen Ryan,[1,2,3]*† Rebecca S. Shapiro,[2]* Christoph F. Kurat,[1,3] David Mayhew,[4] Anastasia Baryshnikova,[1,2,3] Brian Chin,[5] Zhen-Yuan Lin,[6] Michael J. Cox,[1,2,3] Frederick Vizeacoumar,[6] Doris Cheung,[1,3] Sondra Bahr,[1,3] Kyle Tsui,[3,7] Faiza Tebbji,[8,9] Adnane Sellam,[8,10]‡ Fabian Istel,[11] Tobias Schwarzmüller,[11] Todd B. Reynolds,[12] Karl Kuchler,[11] David K. Gifford,[5,13] Malcolm Whiteway,[8,9] Guri Giaever,[2,3,7] Corey Nislow,[1,2,3] Michael Costanzo,[1,3] Anne-Claude Gingras,[2,6] Robi David Mitra,[4] Brenda Andrews,[1,2,3] Gerald R. Fink,[5,13]§ Leah E. Cowen,[2]§ Charles Boone[1,2,3]§

The dimorphic switch from a single-cell budding yeast to a filamentous form enables *Saccharomyces cerevisiae* to forage for nutrients and the opportunistic pathogen *Candida albicans* to invade human tissues and evade the immune system. We constructed a genome-wide set of targeted deletion alleles and introduced them into a filamentous *S. cerevisiae* strain, Σ1278b. We identified genes involved in morphologically distinct forms of filamentation: haploid invasive growth, biofilm formation, and diploid pseudohyphal growth. Unique genes appear to underlie each program, but we also found core genes with general roles in filamentous growth, including *MFG1* (*YDL233w*), whose product binds two morphogenetic transcription factors, Flo8 and Mss11, and functions as a critical transcriptional regulator of filamentous growth in both *S. cerevisiae* and *C. albicans*.

Saccharomyces cerevisiae can undergo a reversible developmental transition from a single-cell budding yeast form into a multicellular filamentous form (*1*). This dimorphic switch enables haploid cells to invade agar in response to carbon deprivation (haploid invasive growth) (*2*, *3*) and to form biofilms on semisolid medium (*4*), whereas diploid cells form chains of elongated cells called pseudohyphae in response to nitrogen starvation (*5*). In the opportunistic pathogen *Candida albicans*, the capacity to transition between yeast and filamentous growth is correlated to virulence (*6*). Because some of the key *S. cerevisiae* signaling pathways that control filamentous growth are highly conserved in *C. albicans* and other more distantly related fungi (*6*), *S. cerevisiae* provides a model system for the identification of genes controlling fungal dimorphism and pathogenesis.

S. cerevisiae filamentous growth is regulated by the nutrient-sensing cyclic adenosine monophosphate (cAMP)–protein kinase A (PKA) pathway (*5*, *7*, *8*) and a mitogen-activated protein kinase (MAPK) pathway (*9*, *10*), whose signals converge on *FLO11* (*MUC1*), a downstream effector of both pathways (*11*). *FLO11* encodes a cell-surface protein that mediates haploid invasive growth, biofilm formation, and diploid pseudohyphal growth phenotypes (*12*, *13*). The *FLO11* promoter is controlled by numerous transcriptional regulators—including Rim101, which is regulated by a complex signaling pathway that also responds to pH stress (*14*); the PKA-regulated transcription factor Flo8 (*11*); the MAPK-regulated transcription factor complex Ste12/Tec1 (*11*, *15*); as well as the transcription factor Mss11 that is regulated by both the PKA and the MAPK signal transduction cascades (*16*). Our understanding of the diverse signals affecting the *FLO11* promoter remains incomplete. Further, the emerging complexities of this regulatory circuitry and others governing filamentous growth necessitate functional genomic analysis of the dimorphic switch.

We amplified a genome-wide set of deletion alleles from the S288c reference strain deletion mutant collection (*17*) with each deletion construct carrying ~200 base pairs (bp) of flanking DNA for efficient integration and gene replacement. This enabled us to construct a set of gene deletions in the *S. cerevisiae* strain Σ1278b, which, unlike S288c, is competent for filamentous growth (*5*). We generated heterozygous diploid deletion mutants and viable haploid mutants of both mating types, which were then mated together to produce homozygous diploid deletion mutants. In total, we covered ~90% of the strains in the S288c reference collection (table S1) (*18*). Because the Σ1278b and S288c genomes are closely related, most deletion mutants should show a similar phenotype; however, some genes may exhibit a background-specific or conditional phenotype (*19*). We compared a subset of the Σ1278b and S288c haploid deletion mutants and found that 267 of 298 mutants tested (~90%) exhibited consistent phenotypes in the two strain backgrounds (table S2) (*18*).

We screened the Σ1278b deletion mutant collection (Fig. 1 and table S3) and identified 577, 700, and 688 genes, including many of the well-characterized filamentous growth genes, with potential roles in haploid invasive growth, pseudohyphal growth, and biofilm development, respectively (table S3). Although haploid invasive growth and biofilm formation were significantly correlated with fitness ($r^2 = 0.19$ and $r^2 = 0.26$, respectively; $P << 10^{-100}$, *t* test relative to random distribution; fig. S1), the majority of mutants identified in these assays (67% haploid invasive growth mutants and 64% biofilm mutants) are not slow growing, suggesting that these genes have roles in filamentous growth that do not affect fitness.

We also screened two *C. albicans* deletion mutant collections for filamentous growth defects (*20*, *21*). One collection is based on genes encoding transcription factors (*20*), another spans genes involved in a range of different cellular processes (*21*), and they combine to cover ~13% of the genome. The mutants were scored for enhanced filamentation under conditions that favor yeast-form growth and for reduced filamentation under filament-inducing conditions (fig. S2). In total, 151 of 829 (~18%) of *C. albicans* mutants had altered filamentation in at least one condition (table S4), a hit rate similar to our *S. cerevisiae* screen. We tested whether *C. albicans* orthologs of the *S. cerevisiae* morphogenetic regulators identified in our Σ1278b screen were enriched for altered filamentation phenotypes and found 104 of the Σ1278b *S. cerevisiae* genes that influence morphogenesis with *C. albicans* orthologs; 43 of 104 (~41%) of these mutants had altered filamentation (table S4), with significant enrichment for morphogenetic regulators ($P < 0.0001$, χ^2 test).

We identified genes required specifically for each one of the developmental programs, including polyamine biosynthetic genes (Fig. 2), required for biosynthesis of spermine, which were required only for pseudohyphal growth and whose defect was rescued by exogenous spermine (fig. S3). We focused on a set of 61 genes required for all three filamentous growth programs (defined as "core" genes) (Fig. 2 and table S3). Notably, the deletion mutants for the majority of core genes with previously unknown roles in filamentous growth were reconstructed and retested for similar phenotypes. Haploid invasive growth and biofilm formation phenotypes were confirmed for 43/46 (93%) and 45/46 (98%) of haploid mutants tested, respectively (table S5). Moreover,

[1]Banting and Best Department of Medical Research, University of Toronto, Toronto, ON M5S 3E1, Canada. [2]Department of Molecular Genetics, University of Toronto, Toronto, ON M5S 1A8, Canada. [3]Terrence Donnelly Centre for Cellular and Biomolecular Research, University of Toronto, Toronto, ON M5S 3E1, Canada. [4]Department of Genetics and Center for Genome Sciences and Systems Biology, Washington University, School of Medicine, St. Louis, MO 63108, USA. [5]Whitehead Institute for Biomedical Research, Cambridge, MA 02142, USA. [6]Samuel Lunenfeld Research Institute, Mount Sinai Hospital, Toronto, ON M5G 1X5, Canada. [7]Department of Pharmacy, University of Toronto, Toronto, ON M5S 3E1, Canada. [8]Biotechnology Research Institute, National Research Council of Canada, Montréal, QC H4P 2R2, Canada. [9]Department of Biology, McGill University, Montréal, QC H3A 1B1, Canada. [10]Department of Anatomy and Cell Biology, McGill University, Montréal, QC H3A 1B1, Canada. [11]Medical University Vienna, Christian Doppler Laboratory for Infection Biology, Max F. Perutz Laboratories, Campus Vienna Biocenter, A-1030 Vienna, Austria. [12]Department of Microbiology, University of Tennessee, Knoxville, TN 37996, USA. [13]Broad Institute of MIT and Harvard University, Cambridge, MA 02142, USA.

*These authors contributed equally to this work.
†Present address: Energy Biosciences Institute, University of California Berkeley, Berkeley, CA 94720, USA.
‡Present address: Institute for Research in Immunology and Cancer (IRIC), University of Montreal, Montréal, QC H3T 1J4, Canada.
§To whom correspondence should be addressed. E-mail: charlie.boone@utoronto.ca (C.B.); leah.cowen@utoronto.ca (L.E.C.); gfink@wi.mit.edu (G.R.F.)

the pseudohyphal growth phenotype was also confirmed for all 16 homozygous diploid mutants tested (table S5). *FLO11* is critical for all forms of filamentous growth, and a number of the core genes code for proteins that regulate *FLO11* expression, including three components of the Rpd3L histone deacetylase complex, 10 members of the Rim101 signaling pathway, and four *FLO11* transcriptional regulators: Mit1, Tec1, Flo8, and Mss11.

The core filamentous growth set also contained a previously uncharacterized gene, *MFG1* (*YDL233W*) (Fig. 2). The relative expression of a *FLO11pr-GFP* reporter, in which the *FLO11* promoter drives the expression of green fluorescent protein (GFP), enabled us to test genes for roles in *FLO11* expression. Indeed, in a colony assay, deletion mutants of known positive regulators of *FLO11* expression exhibited reduced *FLO11pr-GFP* expression, whereas *dig1*Δ cells, which lack a negative regulator, showed increased *FLO11pr-GFP* expression (Fig. 3A and fig. S4). Similar results were observed in a biofilm assay (fig. S4). The *mfg1*Δ deletion mutant also showed reduced *FLO11pr-GFP* expression (Fig. 3A) and exhibited extreme phenotypes in our quantitative filamentous growth assays, similar to the phenotype associated with the deletion mutants of *FLO8* and *MSS11*, which encode important transcriptional regulators of filamentous growth (Fig. 1 and table S3).

Consistent with a filamentous growth transcriptional regulatory role, we found that an Mfg1-GFP fusion protein localized to the nucleus in Σ1278b cells (fig. S5). Although Mfg1 does not contain a characterized DNA-binding motif, Mfg1 physically interacts with Flo8 and Mss11, which bind directly to the *FLO11* promoter (Fig. 3B). Furthermore, chromatin immunoprecipitation (chIP) analysis demonstrated that Mfg1 associates with the *FLO11* promoter in a region that overlaps with the Flo8-binding domain (–1.1 kb from the AUG codon), and it does so in a Flo8- and Mss11-dependent manner (Fig. 3C). chIP analysis also showed that the binding of Flo8 and Mss11 to the *FLO11* promoter was reduced in the absence of Mfg1, suggesting that Mfg1 may control *FLO11* gene expression as part of a promoter-bound complex with Flo8 and Mss11.

In order to assess the global spectrum of genes regulated by Mfg1, Flo8, and Mss11, we performed calling-card analysis, which identifies promoters bound by transcription factors in vivo (*18*, *22*). At a *P* value cutoff of 10^{-4}, 154 promoters were bound significantly by Mfg1, 174 bound by Flo8, and 268 bound by Mss11 (table S6). In total, 136 of the Mfg1-bound promoters overlapped those bound by Flo8 ($P < 6.4 \times 10^{-226}$, hypergeometric test), and 118 of the Mfg1-bound promoters overlapped those bound by Mss11 ($P < 2.2 \times 10^{-128}$, hypergeometric test), with 111 Mfg1-bound promoters overlapping with both Flo8 and Mss11 (Fig. 3D). Mfg1, Flo8, and Mss11 all directed calling cards to the *FLO11* promoter as well as promoters of genes involved in *FLO11* expression, and 45 of the Mfg1-, Flo8-, and Mss11-bound promoters regulate genes that lead to filamentous growth phenotypes when deleted. We performed calling-card analysis in a Flo8-tagged *mfg1*Δ strain and a

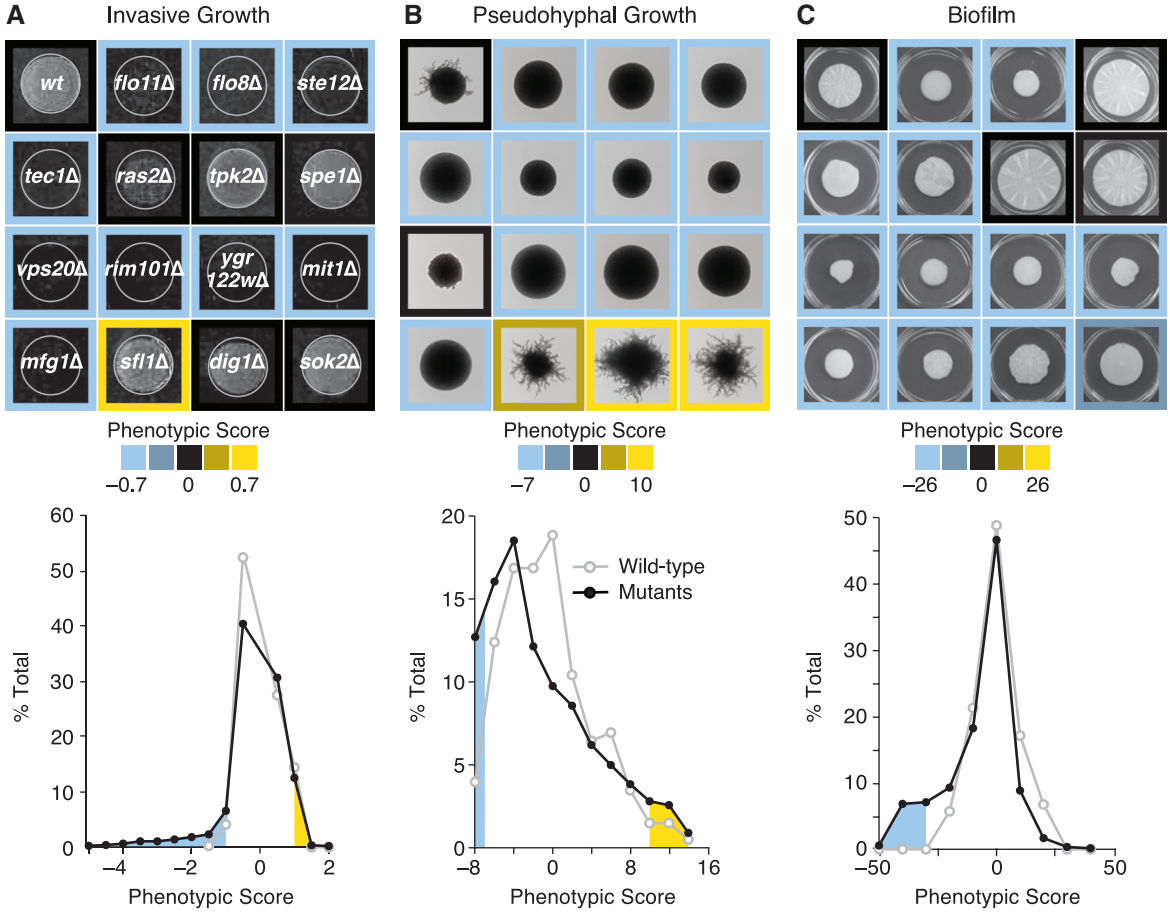

Fig. 1. (**A**) (Top) Haploid invasive growth mutants after plate wash and regrowth; (bottom) distribution of quantitative phenotypes. Mutants with a phenotypic score ≤ –0.7 or ≥ 0.7 were classified as hypoinvasive or hyperinvasive, respectively (*18*). (**B**) (Top) Pseudohyphal growth mutants after 5 days growth on SLAD medium; (bottom) distribution of quantitative pseudohyphal growth phenotypes. Mutants with scores ≤ –7 were classified as hypopseudohyphal, whereas scores ≥ 10 were considered to have a hyperpseudohyphal phenotype (*18*). (**C**) (Top) Biofilm mat-forming mutants after 5 days growth on 0.3% agar; (bottom) distribution of quantitative biofilm formation phenotypes. Mutants with scores ≤ –26 were classified as hypopseudohyphal, whereas scores ≥ 26 were considered to have a biofilm formation phenotype (*18*). The fraction of mutants with hypoactive phenotypic scores is shown in blue, and the fraction of mutants with hyperactive scores is shown in yellow.

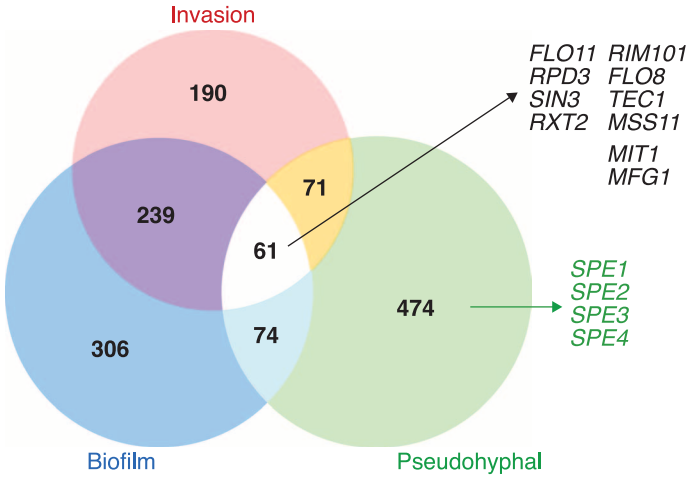

Fig. 2. Venn diagram of the total number of mutants tested in all three phenotypic assays that showed significant dimorphism phenotypes. Examples of core genes required for all three phenotypes and polyamine biosynthetic genes required specifically for pseudohyphal growth are highlighted.

Mfg1-tagged *flo8*Δ strain, such that the tagged protein is assessed for target binding in the absence of the other transcription factor (table S7), and found that the global fraction of target genes that showed reduced binding were 98.6% and 90.8% of those identified for Mfg1 (Fig. 3E) and Flo8 (fig. S6), respectively.

To assess the extent to which Mfg1 contributes to *FLO11* expression, we examined pseudohyphal growth in double mutants. We combined deletion alleles that are defective for negative regulators of *FLO11* expression, including *sfl1*Δ, *dig1*Δ, and *sok2*Δ, with deletion alleles of signaling molecules and transcriptional activators that control *FLO11* expression. This generated a double-mutant epistasis profile for each of the deletion alleles and revealed that *mfg1*Δ and *mss11*Δ suppress the hyperfilamentation phenotypes associated with each of the three negative regulators (Fig. 3F). Thus, Mfg1 appears to function like Mss11 as a critical regulator of filamentous growth.

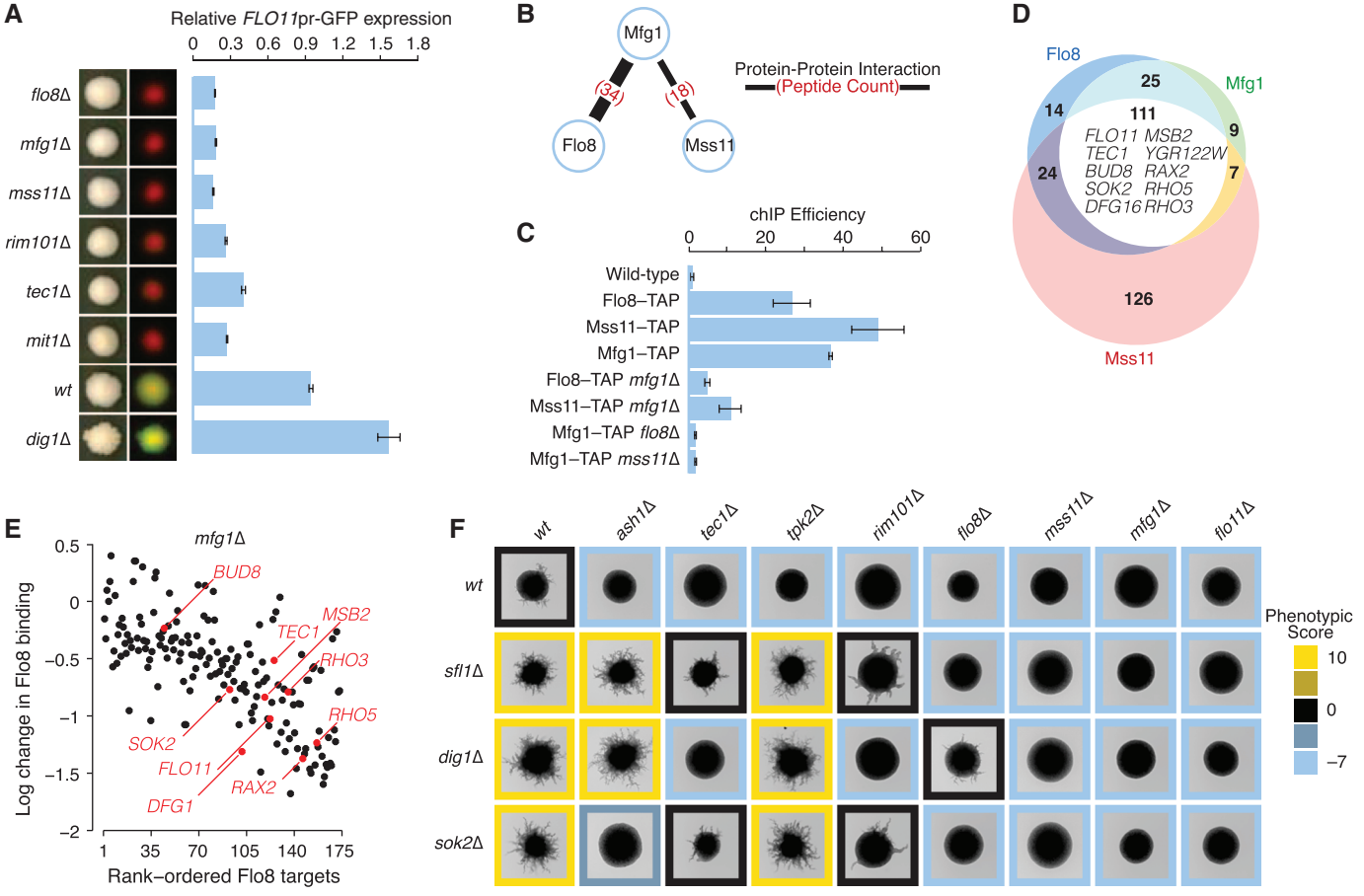

Fig. 3. (**A**) Expression of *FLO11pr-GFP* relative to *RPL39B-RFP* in haploid deletion mutants grown for 4 days on 2% agar. (**B**) Mfg1 physically interacts with Flo8 and Mss11 in Σ1278b cells as determined by coimmunoprecipitation coupled with mass spectrometry. (**C**) chIP of Mfg1, Mss11, and Flo8 at −1.1 kb of the *FLO11* promoter. Error bars indicate SEM. (**D**) Venn diagram depicts the overlap of promoter enrichment by Mfg1, Mss11, and Flo8 assessed by calling-card analysis. (**E**) Decreased levels of Flo8 target gene interactions as measured by calling-card analysis in *mfg1*Δ mutant versus wild-type cells. (**F**) Double homozygous diploid mutant phenotypes for genes that affected pseudohyphal growth. Single mutants annotated with a hyperfilamentous phenotype are listed on the vertical axis, and single mutants annotated with a hypofilamentous phenotype are on the horizontal axis. Double mutants exhibiting no, a hypofilamentous, or a hyperfilamentous phenotype relative to the single mutant control are highlighted by black, blue, and yellow squares, respectively.

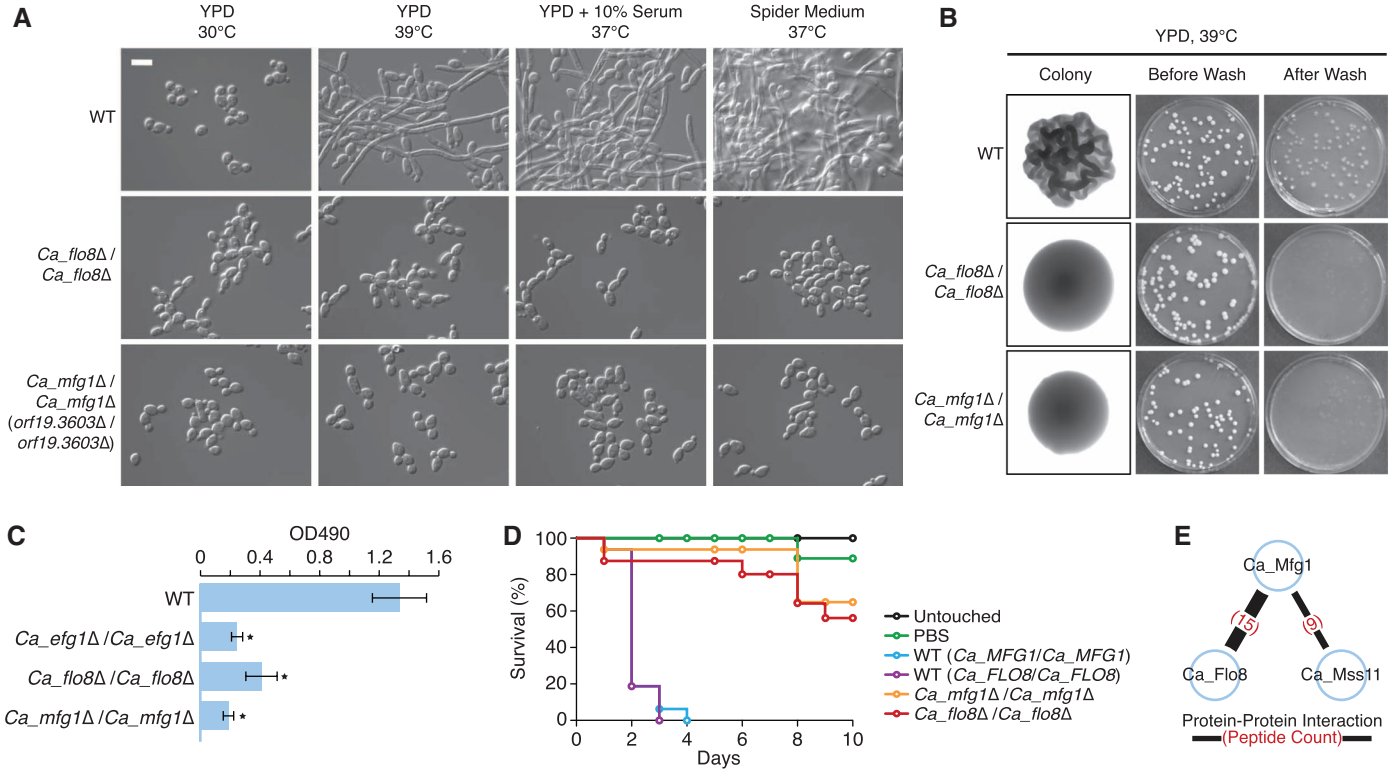

Fig. 4. (**A**) Morphology of cells grown in liquid yeast extract, peptone, and dextrose medium (YPD) at 30°C for 8 hours or under different filament-inducing conditions, as indicated. (**B**) Cells were plated on YPD agar and grown at 39°C for 5 days to assess colony morphology. (**C**) Biofilms were grown in standard *C. albicans* RPMI growth conditions, and metabolic activity was quantified. Error bars indicate SEM. (**D**) Virulence of indicated *C. albicans* strains was tested in a *G. mellonella* survival model of pathogenesis. (**E**) Ca_Mfg1 physically interacts with Ca_Flo8 and Ca_Mss11 in *C. albicans* cells as determined by coimmunoprecipitation coupled with mass spectrometry.

If *MFG1* is a conserved regulator of filamentous growth, then the orthologous gene encoding a similar protein in *C. albicans* should have a role in dimorphism and pathogenicity. The previously uncharacterized gene *Ca_MFG1* (*orf19.3603*) is the ortholog of *S. cerevisiae MFG1* but was absent from the examined *C. albicans* mutant libraries. Deletion of *Ca_MFG1* blocked filamentation and invasive growth in response to numerous environmental cues, similar to deletion of *Ca_FLO8* (Fig. 4A, B). The homozygous diploid *Ca_mfg1Δ/Ca_mfg1Δ* deletion mutant was also defective in the formation of biofilms (Fig. 4C), resembling the phenotype of mutants lacking *Ca_FLO8* or *Ca_EFG1* (Fig. 4C), both of which are known to be critical for this process (*6*). Consistent with the importance of morphogenetic plasticity for virulence, the *Ca_mfg1Δ/Ca_mfg1Δ* mutant had decreased virulence in the greater wax moth *Galleria mellonella* infection model (Fig. 4D). Complementation of the *Ca_mfg1Δ/Ca_mfg1Δ* mutant with a wild-type *Ca_MFG1* allele restored wild-type phenotypes (fig. S7). Lastly, we analyzed Ca_Mfg1 protein interactions and found that Ca_Mfg1 physically interacts with Ca_Flo8 and Ca_Mss11 (Fig. 4E and tables S8 and S9). These findings highlight conserved cellular circuitry controlling filamentous growth and identify Ca_Mfg1 as a previously unknown component of the *C. albicans* Flo8-Mss11 complex, which is integral for filamentous morphogenesis (*23*, *24*). We conclude that systematic genetic analyses of diverse *S. cerevisiae* strains provides a powerful and general approach to identify not only the function of previously uncharacterized genes within this model system but also the function of orthologous genes across distantly related yeast strains, including our understanding of filamentation in fungal pathogens.

References and Notes

1. R. J. Bastidas, J. Heitman, *Proc. Natl. Acad. Sci. U.S.A.* **106**, 351 (2009).
2. P. J. Cullen *et al.*, *Genes Dev.* **18**, 1695 (2004).
3. P. J. Cullen, G. F. Sprague Jr., *Proc. Natl. Acad. Sci. U.S.A.* **97**, 13619 (2000).
4. T. B. Reynolds, G. R. Fink, *Science* **291**, 878 (2001).
5. C. J. Gimeno, P. O. Ljungdahl, C. A. Styles, G. R. Fink, *Cell* **68**, 1077 (1992).
6. R. S. Shapiro, N. Robbins, L. E. Cowen, *Microbiol. Mol. Biol. Rev.* **75**, 213 (2011).
7. X. Pan, J. Heitman, *Mol. Cell. Biol.* **22**, 3981 (2002).
8. K. B. Lengeler *et al.*, *Microbiol. Mol. Biol. Rev.* **64**, 746 (2000).
9. H. U. Mösch, R. L. Roberts, G. R. Fink, *Proc. Natl. Acad. Sci. U.S.A.* **93**, 5352 (1996).
10. H. D. Madhani, C. A. Styles, G. R. Fink, *Cell* **91**, 673 (1997).
11. S. Rupp, E. Summers, H. J. Lo, H. Madhani, G. Fink, *EMBO J.* **18**, 1257 (1999).
12. W. S. Lo, A. M. Dranginis, *Mol. Biol. Cell* **9**, 161 (1998).
13. B. Guo, C. A. Styles, Q. Feng, G. R. Fink, *Proc. Natl. Acad. Sci. U.S.A.* **97**, 12158 (2000).
14. K. J. Barwell, J. H. Boysen, W. Xu, A. P. Mitchell, *Eukaryot. Cell* **4**, 890 (2005).
15. H. D. Madhani, G. R. Fink, *Science* **275**, 1314 (1997).
16. D. van Dyk, I. S. Pretorius, F. F. Bauer, *Genetics* **169**, 91 (2005).
17. E. A. Winzeler *et al.*, *Science* **285**, 901 (1999).
18. Materials and methods are available as supplementary materials on *Science* Online.
19. R. D. Dowell *et al.*, *Science* **328**, 469 (2010).
20. O. R. Homann, J. Dea, S. M. Noble, A. D. Johnson, *PLoS Genet.* **5**, e1000783 (2009).
21. S. M. Noble, S. French, L. A. Kohn, V. Chen, A. D. Johnson, *Nat. Genet.* **42**, 590 (2010).
22. H. Wang, D. Mayhew, X. Chen, M. Johnston, R. D. Mitra, *Genome Res.* **21**, 748 (2011).
23. F. Cao *et al.*, *Mol. Biol. Cell* **17**, 295 (2006).
24. C. Su, Y. Li, Y. Lu, J. Chen, *Eukaryot. Cell* **8**, 1780 (2009).

Acknowledgments: We thank M. Johnston for inspiring the calling-card analysis and M. Usaj for assistance with image and data processing. Supported by the Canadian Institutes of Heath Research (MOP-97939) (C.B. and B.A.), Natural Sciences and Engineering Research Council (NSERC) of Canada (RGPIN 204899-05) (C.B.), Howard Hughes Medical Institute Research Scholar (C.B.), Career Award in the Biomedical Sciences from the Burroughs Wellcome Fund (L.E.C.), Canada Research Chair in Microbial Genomics and Infectious Disease (L.E.C.), NSERC Discovery Grant (355965-2009) (L.E.C.), and NIH (GM40266 and GM035010) (G.R.F.). C.N. and G.G. are supported by a grant from the National Human Genome Research Institute. R.S.S. is supported by an NSERC Canada Graduate Scholarship. C.F.K. is supported by a European Molecular Biology Organization long-term fellowship Raw images and data derived from haploid invasive growth, pseudohyphal growth and biofilm formation assays can be downloaded from http://spidey.ccbr.utoronto.ca/data/ryan_et_al/.

Supplementary Materials

www.sciencemag.org/cgi/content/full/337/6100/1353/DC1
Materials and Methods
Figs. S1 to S7
References (*25*–*41*)

7 May 2012; accepted 16 July 2012
10.1126/science.1224339